

Multiphoton imaging of ultrashort pulse laser ablation in the intracellular parasite *Theileria*

Patrick Stoller

Dominik Marti

University of Bern
Institute of Applied Physics
Sidlerstrasse 5
Bern, Switzerland

Jacqueline Schmuckli-Maurer

Dirk Dobbelaere

Division of Molecular Pathobiology
Department of Clinical Research and VPH
Vetsuisse Faculty Bern
Länggassstrasse 122
Bern, Switzerland

Martin Frenz

University of Bern
Institute of Applied Physics
Sidlerstrasse 5
Bern, Switzerland

Abstract. *Theileria annulata* is an intracellular parasite that infects and transforms bovine leukocytes, inducing continuous proliferation of its host cell both *in vivo* and *in vitro*. *Theileria*-infected cells can easily be propagated in the laboratory and serve as a good model for laser ablation studies. Using single pulses from an amplified ultrashort pulse laser system, we developed a technique to introduce submicrometer holes in the plasma membrane of the intracellular schizont stage of *Theileria annulata*. This was achieved without compromising either the viability of the organisms or that of the host cell that harbors the parasite in its cytoplasm. Multiphoton microscopy was used to generate image stacks of the parasite before and after ablation. The high axial resolution allowed precise selection of the region of the membrane that was ablated. It also allowed observation of the size of the holes generated (in fixed, stained cells) and determination of the structural changes in the parasite resulting from the laser pulses (in living cells *in vitro*). This technique opens a new possibility for the transfection of *Theileria* or delivery of molecules to the schizont that may prove useful in the study of this special host-parasite relationship. © 2008 Society of Photo-Optical Instrumentation Engineers. [DOI: 10.1117/1.2960524]

Keywords: laser nanosurgery; multiphoton microscopy; *Theileria*; intracellular parasite; ultrashort pulse laser; optoporation.

Paper 07243RR received Jul. 6, 2007; revised manuscript received Mar. 11, 2008; accepted for publication Mar. 14, 2008; published online Aug. 8, 2008.

1 Introduction

Intracellular protozoan parasites such as *Plasmodium* and *Toxoplasma* reside in a parasitophorous vacuole, a membrane-bound organelle that is often specifically modified to accommodate the invading organism. Other parasites such as *Theileria* or *Trypanosoma cruzi* are found free in the host cell cytoplasm, where they interfere directly with the host cell to ensure their long-term persistence.¹

Theileria parasites, in particular *T. parva* and *T. annulata*, possess the unique capacity to transform the cells they infect, inducing uncontrolled proliferation of the infected cells, which spread rapidly through the body of the infected animal. They cause economically important diseases of cattle (called East Coast fever and Tropical Theileriosis, respectively) in East and Northern Africa, the Middle East, and large areas of Asia.

Theileria-transformed cells take on many properties of tumor cells.² As discussed in two recent reviews,^{3,4} the direct contact with host cell components allows the *Theileria* schizont to interfere in a unique manner with the host cell's signaling pathways that regulate host cell proliferation and survival,⁵⁻⁷ resulting in continuous proliferation of parasite-harboring cells and protection against apoptosis.^{8,9} Despite the fact that considerable progress has been made identifying the signaling pathways involved, the molecular interactions

between *Theileria* and its host cell are still poorly understood and difficult to study. Being an obligate intracellular organism, tools are largely lacking that facilitate the entry of molecules that normally do not cross the parasite membrane such as resident host cell molecules, molecules that have been taken up by the host cell, or molecules that were introduced into the host cells by transfection. Lacking a method to transfect the schizont stage of the parasite, it is difficult to gain detailed insight into the molecular mechanism by which the parasite gains control over a host cell. The recent completion of the genomic sequence of *T. parva*¹⁰ and *T. annulata*¹¹ further highlights the importance of the development of such a technique.

While transient transfection has been achieved for *Theileria* sporozoites, these cannot be cultured, and elaborate facilities to house both infected calves and the ticks that transmit the parasite are required to produce them.¹² The schizont stage of *Theileria*, on the other hand, resides in the continuously proliferating host cells and can be propagated indefinitely by *in vitro* culture. Conventional methods for transfection, such as electroporation, and also microinjection have not yet been successful in the schizont. Ultrashort pulse laser ablation to generate small holes in the membrane has recently been used successfully to transfect cells.^{13,14} If applicable to schizont membranes, this technique could pave the way for the development of a novel method to transfect *Theileria*. This method can be combined with multiphoton microscopy to enable

Address all correspondence to: Prof. Martin Frenz, Institute of Applied Physics, University of Bern, Sidlerstrasse 5, Bern, Switzerland. Tel: +41 31 631 8943; Fax: +41 31 631 3765; E-mail: martin.frenz@iap.unibe.ch.

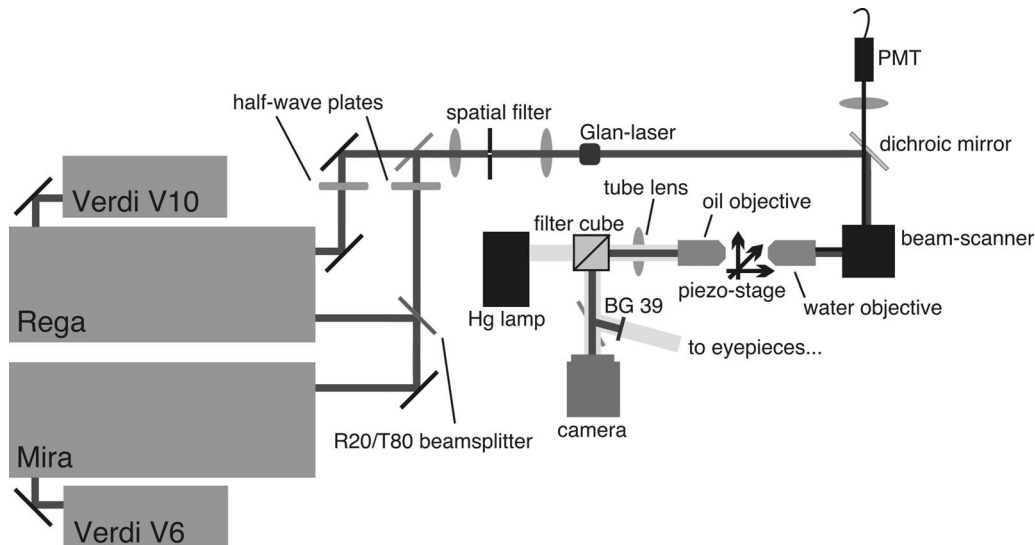


Fig. 1 Sketch of the experimental setup. Refer to the text for details.

precise selection of the regions of the sample that are ablated and to image structural changes in the parasite and in the cell in three dimensions.

Multiphoton fluorescence microscopy is a powerful method to obtain three-dimensional (3-D) images of biological samples and has found growing use in biophysics and biology laboratories around the world.^{15,16} In a multiphoton microscope, a high-intensity laser beam is tightly focused onto the sample and is raster-scanned with respect to the sample to generate an image. Because the two- (three-) photon fluorescence signal varies as the square (cube) of the laser intensity, it is confined to the focus. This provides images with high axial resolution—comparable to confocal microscopy—but without the need for a confocal pinhole and with significantly reduced photobleaching. The near-infrared (NIR) excitation wavelengths generally used for such scans also penetrate deeper into biological samples and allow imaging at greater depths. In order to achieve the high peak intensities necessary to observe multiphoton effects and to do so while avoiding damage to the sample, ultrashort pulse laser oscillators are used. When focused through a high-numerical-aperture (NA) microscope objective, these lasers provide high peak intensities and at the same time deposit very little energy per pulse into the sample.

By increasing the pulse energy, it is possible to use the same laser to ablate small regions of a sample with a size comparable to or smaller than the resolution of multiphoton microscopy images.¹⁷ Ultrashort pulse laser ablation can be achieved both using single amplified laser pulses and using a train of pulses directly from a high-repetition-rate oscillator. The ablation threshold in the former case is about ten times higher than for the latter, and the physical mechanisms responsible are very different.¹⁸ Ultrashort pulse laser ablation has been used, for example, to make submicrometer cuts in chromosomes¹⁷ and in nervous tissue,^{19,20} to disrupt organelles in a living cell,^{21,22} and to study embryo dynamics.²³

In this work, we seek to determine whether ultrashort pulse laser ablation can be used to generate small holes in the membrane of the intracellular parasite *T. annulata* without compro-

promising the viability of the parasite or the cell. Since conventional epi-fluorescence imaging does not have a high enough axial resolution to permit precise determination of the location of the parasite membrane with respect to the focused laser spot—the parasite is only of the order of a few micrometers in size—we turn to multiphoton microscopy to accurately focus the laser on specific sections of parasite membrane. Changes in the intracellular parasite in response to laser ablation are also difficult to see without a 3-D imaging technique. We first demonstrate the capabilities of this combined technique to generate and visualize submicrometer holes in the parasite membrane in fixed, stained samples. We determine the threshold for visible ablation using single pulses and measure the extent of damage axially and laterally as a function of the pulse energy. We then focus on ablation in living *Theileria* infected macrophages, which express green fluorescent protein, in order to observe the resulting 3-D changes in the structure and organization of the parasite and determine the viability of the treated cells.

2 Experiment

2.1 Microscope Setup

The experimental setup is illustrated in Fig. 1. The laser system used consisted of a Coherent Mira ultrashort pulse laser oscillator and a Coherent RegA regenerative amplifier (Coherent, Inc., Santa Clara, California). The Mira was operated at a wavelength of 800 nm with a repetition rate of 76 MHz and a pulse energy of ~ 10 nJ. The regenerative amplifier was operated in single-pulse mode; seed pulses from the Mira were selected and regeneratively amplified to energies of about 4 μ J. The Mira and the RegA were pumped by a 6-W and a 10-W Coherent Verdi diode-pumped solid-state laser, respectively. The Mira beam was used to perform multiphoton imaging of the samples; the RegA beam was employed to perform laser ablation.

The beams from the Mira and from the RegA were passed through power dividers consisting of a zero-order half-wave plate and a Glan-laser polarizer to allow adjustment of the

laser power. The beams were overlapped before the microscope and passed through a beam expander and spatial filter consisting of two NIR achromatic doublets ($f=100$ mm and $f=150$ mm) and a $25\text{-}\mu\text{m}$ -diameter pinhole. The combined beam was reflected by a dichroic mirror designed for multiphoton microscopy (Omega Optical XF2033, Brattleboro, Vermont) onto the entrance port of a two-axis beam-scanning system (GSI Lumonics, Billerica, Massachusetts). The beam exiting the scanner then passed through the back aperture of the microscope objective (Nikon $60\times$ Fluor 1.0 NA water dipping to image living cells or Nikon $60\times$ Plan Apo 1.2 NA water immersion to image fixed cells; Nikon, Tokyo, Japan) and was focused onto the sample. The beam scanner allowed raster scanning of the focused spot in the x - y plane normal to the optical axis of the objective. The beam diameter was chosen to slightly overfill the back aperture of the microscope objective in order to achieve tight focusing.²⁴ The objectives were mounted above the Zeiss Axiovert 135 inverted microscope (Carl Zeiss AG, Jena, Germany) on a translation stage using a custom-built microscope attachment that replaced the bright-field condenser and illumination tower. During scanning laser microscopy using the Mira laser as the excitation source, the two-photon fluorescence was collected and collimated using the same objective, passed through the dichroic mirror, and weakly focused onto a photomultiplier tube (Hamamatsu H5783, Hamamatsu Photonics, K. K., Hamamatsu City, Japan). During laser ablation experiments using the RegA, unwanted photobleaching was prevented by blocking the Mira beam.

To locate cells of interest and to bring these cells into the vicinity of the focused laser spot, the microscope was operated in wide-field, epi-fluorescence mode with a Zeiss HBO 100 mercury arc lamp and a fluorescent filter cube with excitation, emission, and dichroic filters designed for the fluorophores used—Alexa488 and green fluorescent protein (GFP). A Zeiss $40\times$ 1.3 NA Plan Neofluar objective was mounted in the objective turret. It was used for epi-fluorescence microscopy and also collected transmitted laser light from the objective used for beam scanning, allowing rough positioning of the laser focus onto the sample. A pco.1600 camera (PCO AG, Kelheim, Germany) was installed in the camera port above the eyepieces and used both to view the epi-fluorescence images and to adjust the focus of the Mira and RegA beams. A BG-38 glass filter was placed in front of the camera to attenuate the beams to prevent oversaturation of the camera. BG-39 glass filters (Schott AG, Mainz, Germany) were inserted before the eyepieces to completely block the impinging laser beam.

The sample was mounted on a 3-D piezoelectric translation stage (Physik Instrumente GmbH Model P-562.3CL, Karlsruhe, Germany), which allowed scanning in the axial (z) direction and precise lateral (x - y) positioning of the sample. A Labview program (National Instruments Corporation, Austin, Texas) was developed to interface with a National Instruments NI-DAQ 6259 USB analog-to-digital and digital-to-analog device used for scan signal generation and data collection. The program coordinated the motion of the beam scanner and the piezoelectric stage and collected the photomultiplier tube signal in order to obtain 3-D image stacks. The Labview program also allowed triggering of single shots from the RegA

during laser ablation experiments. The location of the shot was specified by selecting the appropriate location in the multiphoton fluorescence image. The Labview program converted the location of the selected point in the image to commands for the beam scanner to move the focus of the laser beam to this position and triggered the RegA to produce a single amplified shot. Three-dimensional image stacks were obtained with an axial step-size of 250 nm and with a lateral step-size of 100 nm and 83 nm for the 1.0 NA objective and the 1.2 NA objective, respectively (to ensure a sampling spatial frequency above the Nyquist frequency). Pixel scan rates of between 5,000 and 200,000 samples per second were used. Single two-dimensional (2-D) x - y images were also obtained; these were typically performed at the lower scan rates to obtain improved signal-to-noise ratio (SNR).

The peak laser intensity and the laser fluence per pulse in the focus of the microscope objective at the sample were estimated as follows: A Coherent Fieldmaster power meter was used to measure the average laser power at the output of the Mira and the RegA; the latter was placed in its continuous pulsing mode at 250 kHz for mean laser power measurements. The transmission from the laser to a point directly before the microscope objective was determined using a calibrated photovoltaic detector that could be switched in and out of the beam path. Transmission through the objectives was estimated by measuring the power before and after the objectives using the photovoltaic detector. The energy of a single laser pulse was then found by dividing the mean laser power at the focus by the repetition rate. In the case of the RegA, the pulse energy increases when the system is operated in single-pulse mode. The appropriate calibration factor to correct for this was determined to be 1.42 using a Laser Precision RjP-735 pyroelectric detector and an Rj-7100 energy meter (Utica, New York). Measurement of 68 pulses directly at the RegA output resulted in a standard deviation in the pulse energy of 7%. Once the pulse energy in the focus has been determined, information about the temporal width and the spatial distribution of the laser light is required to calculate the peak laser intensity and the pulse fluence. The temporal pulse width was measured routinely directly behind both lasers using a Carpe autocorrelator (APE GmbH, Berlin, Germany) and found to be around 180 fs (full-width at half-maximum, FWHM) for the RegA and 135 fs (FWHM) for the Mira assuming a Gaussian temporal pulse profile. Since group-velocity dispersion in the optics between the laser and the sample can lead to pulse broadening, the pulse width was also measured directly at the sample using an external detector supplied with the Carpe autocorrelator. Pulse broadening due to group velocity dispersion in the system was found to be negligible for the RegA; Mira pulses were broadened by about 20%. The peak intensity and pulse fluence were calculated²⁴ assuming diffraction-limited focusing of the beam by the overfilled microscope objectives [$1/e$ radius = $\lambda/(\pi\text{NA})$]. The beam diameter at the $1/e$ intensity was 510 nm and 420 nm for the 1.0 NA and 1.2 NA objectives, respectively.

2.2 Cell Culture

T. annulata-infected macrophages (cell line TaC12) were cultured at 37°C in Leibovitz 15 medium containing 10% (v/v) heat inactivated fetal calf serum (FCS), 20 mM Hepes (pH

7.1), L-glutamine (2 mM), benzylpenicillin (100 units/ml), streptomycin sulphate (100 $\mu\text{g/ml}$), and 70 $\mu\text{M}\beta$ -mercapthoethanol.

2.3 Electroporation

Plasmid DNA (pmaxGFP containing a GFP variant from *Pontellina plumata*) was isolated with a HiSpeed Plasmid Maxi Kit from Qiagen according to the manufacturer's protocol. *Theileria*-infected macrophages were transfected by electroporation with an Easyject Plus from Equibio under the following conditions: 300 V, 1650 μF , 1540 Ω using 30 μg of plasmid DNA. After transfection, cells were seeded into 35-mm glass-bottom dishes with a 14-mm-diam glass bottom with the same thickness as a standard coverglass (Part. No. P35G-1.5-14-C, MatTek Corp., Ashland, Massachusetts). Living cells were analyzed approximately 24 h after transfection. The transfection efficiency was routinely more than 50%.

2.4 Fixed Cells

1.5×10^5 TaC12 cells were seeded on 12-mm glass coverslips and allowed to settle down overnight. They were subsequently fixed in 4% paraformaldehyde (prepared in PBS) for 10 min and then permeabilized in 0.2% Triton (prepared in PBS) for 5 min. This and all of the following steps were carried out at room temperature. Unspecific binding was blocked with PBS containing 10% heat-inactivated FCS for 10 min. The parasite surface was stained with rabbit anti-TaSP antibody²⁵ (Dr. J. Ahmed, Borstel, Germany) diluted 1:50,000 in PBS containing 10% heat-inactivated FCS and applied for 1 h. Cells were then washed three times with PBS and incubated with the secondary antibody, Alexa488-conjugated goat a-rabbit Ab (Molecular Probes A-11034) diluted 1:1500 in PBS containing 10% heat-inactivated FCS for 1 h. Last, the coverslips were mounted with AF1 Mountant solution (Citifluor Ltd, London) on 35-mm glass-bottom dishes with a 14-mm-diam glass bottom with the thickness of standard coverglass (Part. No. P35G-1.5-14-C, MatTek Corp., Ashland, Massachusetts).

3 Results

We performed laser ablation experiments and obtained 3-D multiphoton microscopy image stacks before and after laser nanosurgery both in living and in fixed and immunostained macrophages hosting *T. annulata* schizonts. Experiments in the fixed cells were designed to observe the direct effect of laser ablation with different pulse energies on the immunostained parasite membrane and to determine the size of the ablated region quantitatively in three dimensions. The protocol chosen for permeabilization of the host cell membrane to allow immunostaining of the parasite membrane was selected to minimize damage to intracellular structures, especially to the parasite and the host cell nuclear membranes. Nonetheless, changes to properties of the parasite membrane due to permeabilization of the host cell, immunolabeling, and fixation are inevitable. Fixed and immunostained samples serve as a good model system in which to test laser ablation and to determine the extent of damage in a sample that preserves the size and the multilobed structure of the parasite but cannot be substituted for measurements in living cells. Measurements carried out using intracellular parasites in living host cells were designed to observe structural changes in both the para-

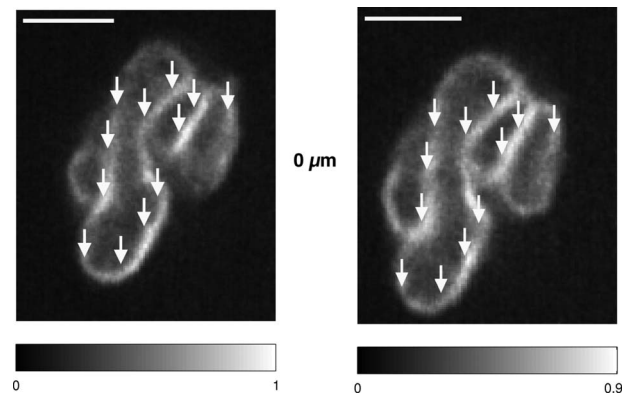


Fig. 2 Images of a fixed and immunostained *Theileria* parasite in the plane normal to the incident laser beam; the scale bar in both images is 2 μm . The images were obtained at a position of $z=0 \mu\text{m}$, the plane where the laser was focused for ablation. The panel on the left (right) shows the cell before (after) ultrashort pulse laser ablation. The arrows point to the locations where single, tightly focused ultrashort pulses irradiated the sample. The peak incident intensity was 5.9 TW/cm^2 . No noticeable change in the parasite is observed.

site and the cell subsequent to laser ablation. In these measurements, the intracellular parasite was observed through its negative contrast against the cytoplasm of the GFP-expressing host cell. The response of living parasites to ultrashort laser pulses of different energies at different times after exposure could be directly determined. The size of the holes generated in the parasite membrane by the laser shot could not be observed in the living parasites because, depending on the pulse energy, they either sealed the hole or changed in structure too rapidly for observation.

Fixed, stained parasites were first imaged using the multiphoton microscope to obtain a three-dimensional image stack. Subsequently, a specific plane within the image stack was chosen for laser ablation experiments. The z position of the piezoelectric translation stage was adjusted to focus the laser in this plane. Specific points in this 2-D image plane were then selected—typically, points lying on the parasite membrane—and exposed to single pulses of controlled energy from the RegA. Then, a second 3-D image stack was obtained using identical scan parameters as the first, allowing direct comparison of the parasites before and after laser exposure.

Figure 2 gives an example of a parasite exposed to peak laser intensities of 5.9 TW/cm^2 (corresponding to a pulse energy of 2.1 nJ). It illustrates that the parasites are composed of several interconnected lobes enclosed by membranes. The arrows in the images point to the locations where the parasite was exposed to laser irradiation. Images are shown at the axial position where the RegA pulses were focused. A comparison of the panel on the left (before laser exposure) and on the right (after laser exposure) shows that no visible damage was induced. Figure 3 shows a parasite exposed to laser pulses with intensities of 18.5 TW/cm^2 (corresponding to a pulse energy of 6.7 nJ). Of the total of eight regions exposed to laser irradiation, one may have been located just outside of the parasite membrane and thus sustained no visible damage; it is labeled in Fig. 3. Three regions show significant changes; they are marked in Fig. 3 and are best visible in the central panels. A magnified view of one such region is shown in the

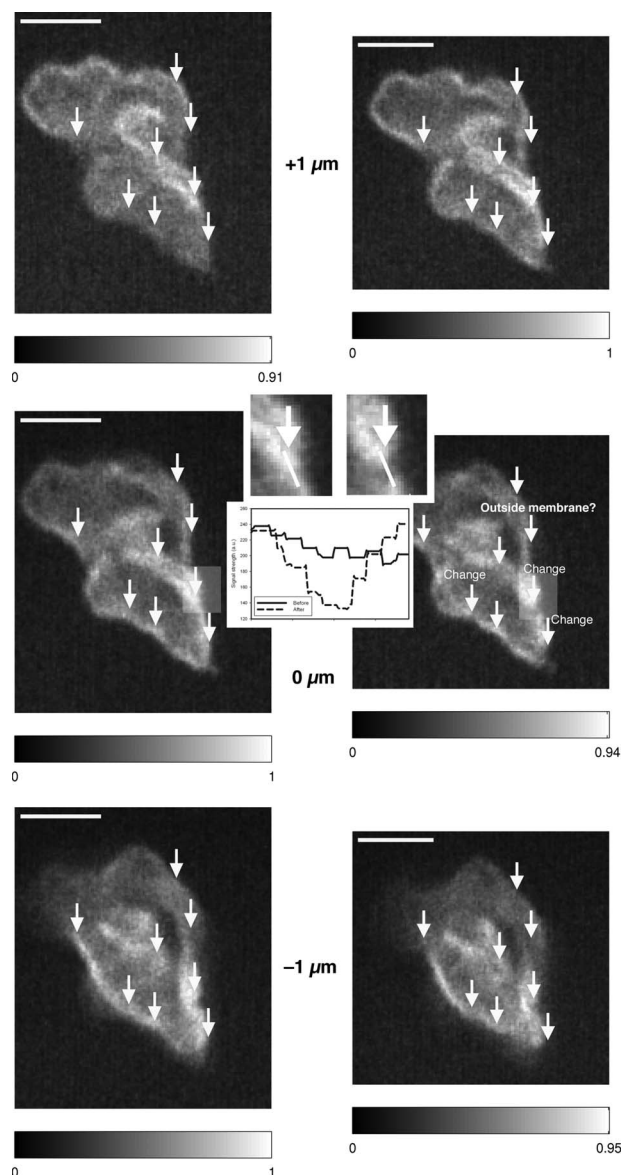


Fig. 3 Selected images of a fixed and immunostained *Theileria* parasite in the plane normal to the incident laser beam; the scale bar in all images is $2\ \mu\text{m}$. From top to bottom, the rows show images at positions $1\ \mu\text{m}$ above, in, and $1\ \mu\text{m}$ below the plane where the laser was focused for ablation. The panels on the left (right) show the cell before (after) ultrashort pulse laser ablation. The arrows point to the locations where single, tightly focused ultrashort pulses irradiated the sample. The peak incident intensity was $18.5\ \text{TW}/\text{cm}^2$, which is above the ablation threshold. Visible changes were generated in the parasite membrane at some points where the laser was focused; these regions (labeled in the figure) extend above and below the plane where ablation was performed by $\sim 1\ \mu\text{m}$. The inset shows a magnified view of one such region and a cross section through an ablated spot; the width of the entire inset is $1\ \mu\text{m}$. One laser shot may have missed the parasite membrane (indicated).

two insets, and a cross section through the damaged region (before and after the laser pulse) is also shown. The damaged zone extends from $z=1.5\ \mu\text{m}$ above the plane where the laser pulses were focused to $z=0.75\ \mu\text{m}$ below and is thus confined to a volume comparable to the focal volume of the laser beam. The lateral extent of visible damage is approximately

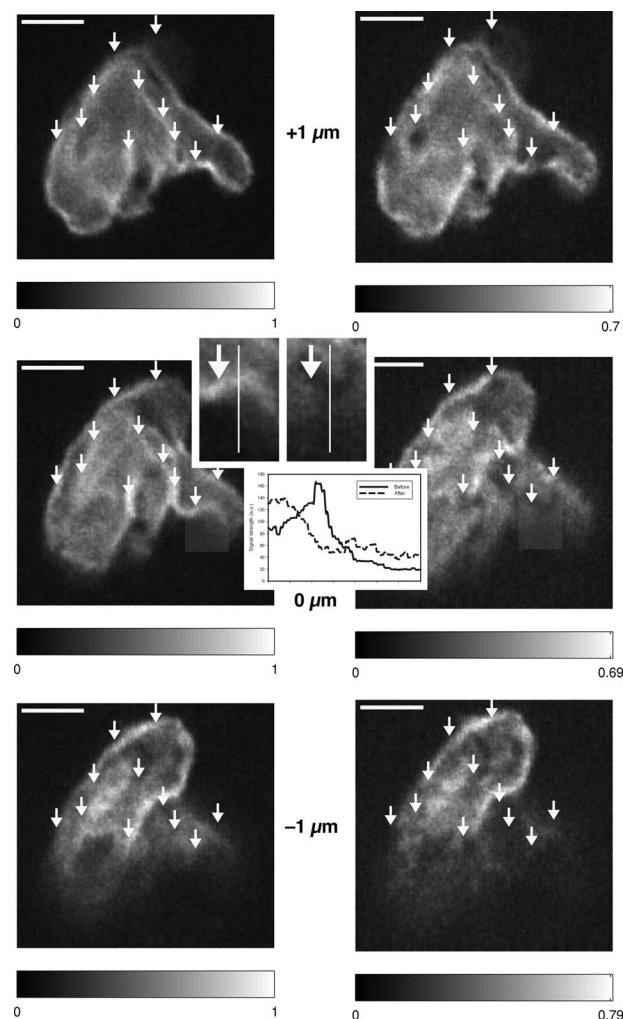


Fig. 4 Selected images of a fixed and immunostained *Theileria* parasite in the plane normal to the incident laser beam; the scale bar in all images is $2\ \mu\text{m}$. From top to bottom, the rows show images at positions $1\ \mu\text{m}$ above, in, and $1\ \mu\text{m}$ below the plane where the laser was focused for ablation. The panels in the left (right) column show the cell before (after) ultrashort pulse laser ablation. The arrows point to the locations where single, tightly focused ultrashort pulses irradiated the sample. The peak incident intensity was $33\ \text{TW}/\text{cm}^2$, which is well above the ablation threshold. Damage is extensive and extends axially from the plane where ablation was performed through the entire parasite. The inset shows a magnified view of one damaged region and a cross section through the ablated spot.

$300\ \text{nm}$. Figure 4 illustrates a parasite exposed to laser pulses with peak intensities ($33\ \text{TW}/\text{cm}^2$, corresponding to a pulse energy of $12\ \text{nJ}$) well above the ablation threshold, where the laser pulses led to complete destruction of parasite lobes. In this case, damage extends through the entire parasite, from $z=2.25\ \mu\text{m}$ above the plane of laser irradiation to $z=1.25\ \mu\text{m}$ below it; the lateral extent of damage is significantly larger than in Fig. 3 but is difficult to determine quantitatively because it spreads beyond the immunostained membrane.

We conducted laser ablation experiments on immunostained parasite membranes at several different ultrashort laser pulse intensities. The results are summarized in Table 1. For pulses with intensities at and below $5.9\ \text{TW}/\text{cm}^2$ (corre-

Table 1 Table of the results of ultrashort pulse laser ablation experiments in fixed, stained parasites. For each peak intensity range, the number of laser shots that resulted in visible damage, in weak bleaching, and in no damage is given. Laser shots that clearly missed the parasite membrane are not taken into account.

Peak laser intensity used for ablation	Number of laser shots	Damage	Weak bleaching	No damage
>0.1 TW/cm ² <6.0 TW/cm ²	68	0	0	68
>9.5 TW/cm ² <19 TW/cm ²	51	4	11	36
>22 TW/cm ² <38 TW/cm ²	42	36	0	6
>50 TW/cm ² <62 TW/cm ²	11	11	0	0
Total	172	51	11	110

sponding pulse energy: 2.1 nJ), we observed no visible change in the parasite membrane (for a total of 68 laser irradiated regions). For pulse with intensities between 9.6 TW/cm² and 18.6 TW/cm² (corresponding to pulse energies between 3.5 nJ and 6.7 nJ), we observed irradiated regions that did not change visibly, irradiated regions where visible holes in the membrane were generated, and regions where the two-photon fluorescence signal became weaker but did not disappear altogether (51 irradiated regions). At these pulse intensities, the lateral extent of visible damage at a given spot was between about 250 nm and 400 nm, while the axial extent was between 1 and 2 μm . For pulses with intensities of 23 TW/cm² up to 61 TW/cm² (53 irradiated regions; corresponding pulse energies: 8.2 nJ to 22 nJ), extensive damage to the parasite occurred in all but six cases. At 23 TW/cm² (corresponding to a pulse energy of 8.2 nJ), the lateral (axial) extent of damage increased to as much as 500 nm, and at 27 TW/cm² (corresponding to a pulse energy of 9.7 nJ), to as much as 800 nm. At higher powers, it was difficult to measure the size of the damaged spot because the damaged regions became irregular and would have extended beyond the parasite.

Subsequent to determining the effect of ultrashort pulse laser irradiation on immunostained parasites, we determined the effect of laser ablation on the parasite-host system in living cells *in vitro*. We first performed control measurements to ensure that the lower peak-power laser light used for multiphoton imaging did not itself lead to damage to the sample; previous studies have reported that this can occur when cells are exposed to high enough pulse energies from an ultrashort pulse oscillator for a long enough time, even when no laser-related damage is immediately visible.²⁶ We found that under the scan conditions used, Mira pulse energies of up to 40 pJ did not result in damage during acquisition of multiphoton image stacks. An isosurface from such an image stack is shown in Fig. 5; two orthogonal cuts through the isosurface allow a view of the interior of the cell. The cell nucleus and

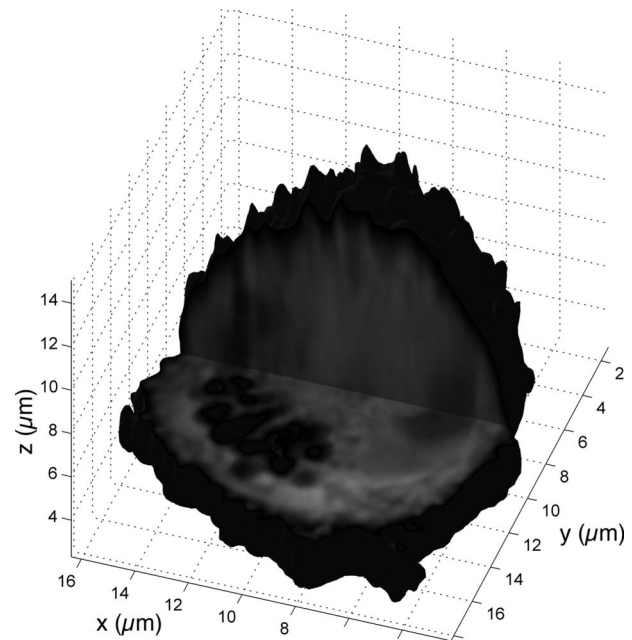


Fig. 5 Isosurface through the 3-D image stack obtained from a multiphoton scan of a living macrophage containing a *Theileria* parasite. The host cell has been transfected with a plasmid coding for GFP. Two orthogonal slices through the cell are shown. The dark lobes of the parasite and the larger, but less dark, kidney-shaped nucleus can be seen.

the parasite are both clearly visible within the cell; one can also observe that the cell spreads out at its base, where it attaches to the coverslip, and takes on a more rounded form as it extends upward. The cell is covered by small hair-like structures (filopodia) that are especially clearly visible at the rounded top surface and are well-resolved by the multiphoton microscopy technique.

Using conventional epi-fluorescence microscopy, we located those macrophage host cells that had both been successfully transfected with a plasmid coding for GFP and contained a *Theileria* parasite. Each selected cell was then imaged to produce a 3-D image stack. Points at the border between the parasite (dark, because of the absence of GFP) and the host cell cytoplasm (bright because of the strong multiphoton fluorescence signal from GFP expressed by the cell) in a 2-D slice through the cell were selected for laser irradiation. Points near the center or the top of parasite lobes were also chosen for laser irradiation. The parasite membrane sometimes runs parallel to the host cell membrane; the points exposed to the laser were chosen to avoid ablating near the membrane of the host cell. Immediately after laser irradiation, a second image stack of the parasite was acquired, a process that required several minutes to complete (each individual image in the stack requires several seconds to acquire). In some cases, subsequent image stacks were also obtained after time intervals of minutes to hours, in order to determine whether there were delayed effects. Figure 6 illustrates the results of an experiment where the laser pulses (11 TW/cm²; corresponding pulse energy: 3.9 nJ) did not result in visible changes. The images on the left (right) show the parasite before (after) exposure to the laser at the depth at which the RegA shots were focused.

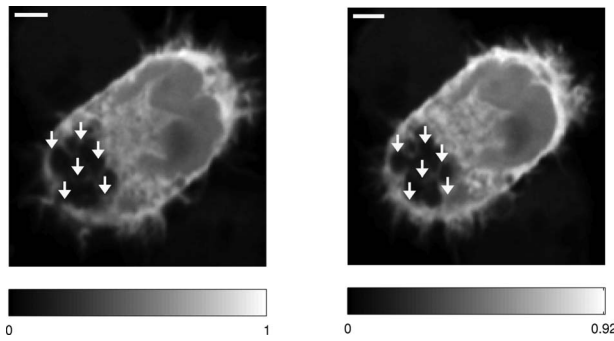


Fig. 6 Images of a live *Theileria* parasite and its macrophage host cell; the scale bar in both images is $2\ \mu\text{m}$. The images are taken in the plane normal to the incident laser beam. The images were obtained at a position of $z=0\ \mu\text{m}$, the plane where the laser was focused for ablation. The panel on the left (right) shows the cell before (after) ultrashort pulse laser ablation. The arrows point to the locations where single, tightly focused ultrashort pulses irradiated the sample. The peak incident intensity was $11\ \text{TW}/\text{cm}^2$. No noticeable change in either the parasite or the cell is observed.

Figure 7 shows a cell before (after) exposure to laser pulses with an intensity around the threshold necessary to produce damage in the parasite membranes of fixed, stained cells (we used $13\ \text{TW}/\text{cm}^2$; corresponding pulse energy: $4.7\ \text{nJ}$). The parasite lobes appear rounder and less dark after ablation. This can be clearly seen in the inset plot of a cross section through the 2-D image and indicates that a signal from GFP can now be detected from within the parasite. Comparing the two central panels in Fig. 7, one observes that no significant photobleaching occurred between the two images; the parasite lobes do not appear brighter simply because of a reduction in contrast. The damage is not necessarily localized exactly to the spot where the laser was focused, as the parasite may change its long-range structure in reaction to laser ablation. In the case of living parasites and host cells, the degree of damage varied significantly from cell to cell. This is illustrated in Figs. 8 and 9, which present seven additional examples of laser-irradiated parasites into which GFP entered. In each figure, the panels on the left (right) show the parasite before (after) laser treatment. For each set of images, a cross section through the image that cuts across the parasite near a location where the laser was focused is given in the center panel. This cross section illustrates more quantitatively the flow of GFP into the parasite lobes. The parasites in Fig. 8 show only subtle changes following laser irradiation. Only individual parasite lobes near the location of one of the laser shots have been filled with GFP. Points along the cross sections through the images that are darker after laser irradiation than before are due to small shifts in the location of the parasite lobes (or of the entire cell) between images; such shifts could sometimes also be observed in cells that were not irradiated. In the examples given in Fig. 9, neighboring parasite lobes are also filled with GFP after laser irradiation. A significant change in the organization of the parasite lobes after laser irradiation is seen in Fig. 9(a). In Fig. 9(c), some of the parasite lobes also become smaller and rounder. A typical pattern seen as a result of laser treatment included the disappearance of single parasite lobes near the location exposed to the laser. These may have been destroyed or may have been filled with enough

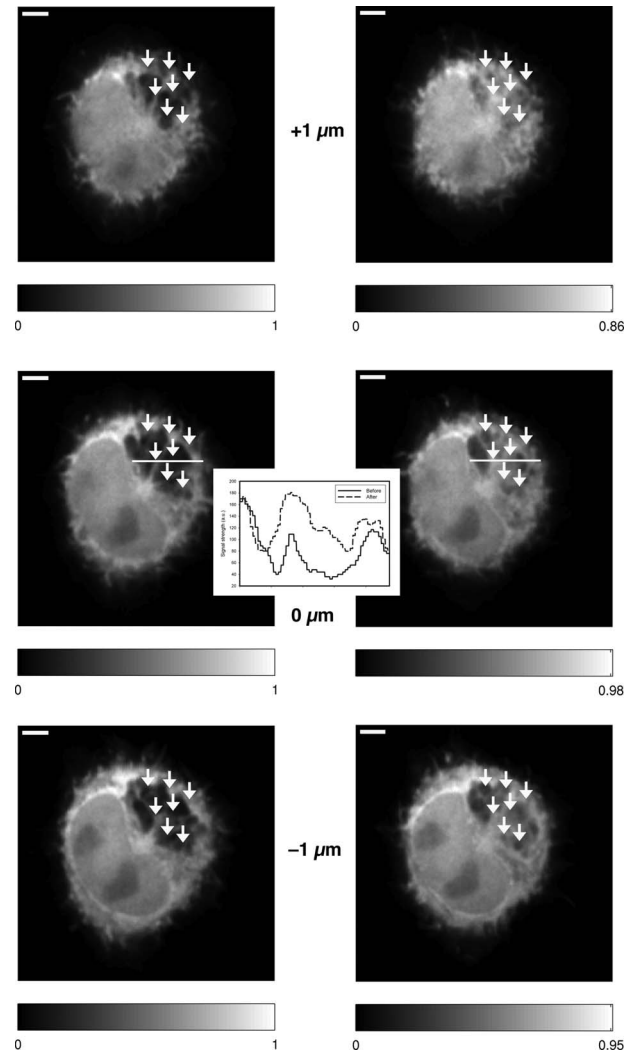


Fig. 7 Images of a live *Theileria* parasite within its macrophage host cell; the scale bar in all images is $2\ \mu\text{m}$. The images are taken in the plane normal to the incident laser beam. From top to bottom, the rows show images at positions $1\ \mu\text{m}$ above, in, and $1\ \mu\text{m}$ below the plane where the laser was focused for ablation. The panels in the left (right) column show the cell before (after) ultrashort pulse laser ablation. The arrows point to the locations where single, tightly focused ultrashort pulses irradiated the sample. The peak incident intensity was $13\ \text{TW}/\text{cm}^2$. The cell shows no large structural changes, but the parasite is significantly altered. Certain parasite lobes have disappeared, and others have changed in shape, becoming rounder. Many lobes have also become less dark, suggesting that they may have filled with GFP present in the surrounding cytoplasm. The inset in the central panel shows a cross section through the image along the white line shown.

GFP to render them indistinguishable from the surrounding host cell cytoplasm [refer, for example, to Fig. 9(c)].

Of a total of 22 cells exposed to peak laser intensities between $8.8\ \text{TW}/\text{cm}^2$ and $25\ \text{TW}/\text{cm}^2$ (chosen based on the the experiments with fixed parasites), 10 parasites were successfully filled with GFP. In some cells, laser intensities as low as $14\ \text{TW}/\text{cm}^2$ (corresponding to a pulse energy of $5.0\ \text{nJ}$) led to cell death, while others remained viable even after exposure to intensities as high as $25\ \text{TW}/\text{cm}^2$ (corresponding to a pulse energy of $8.9\ \text{nJ}$). Intensities lower than

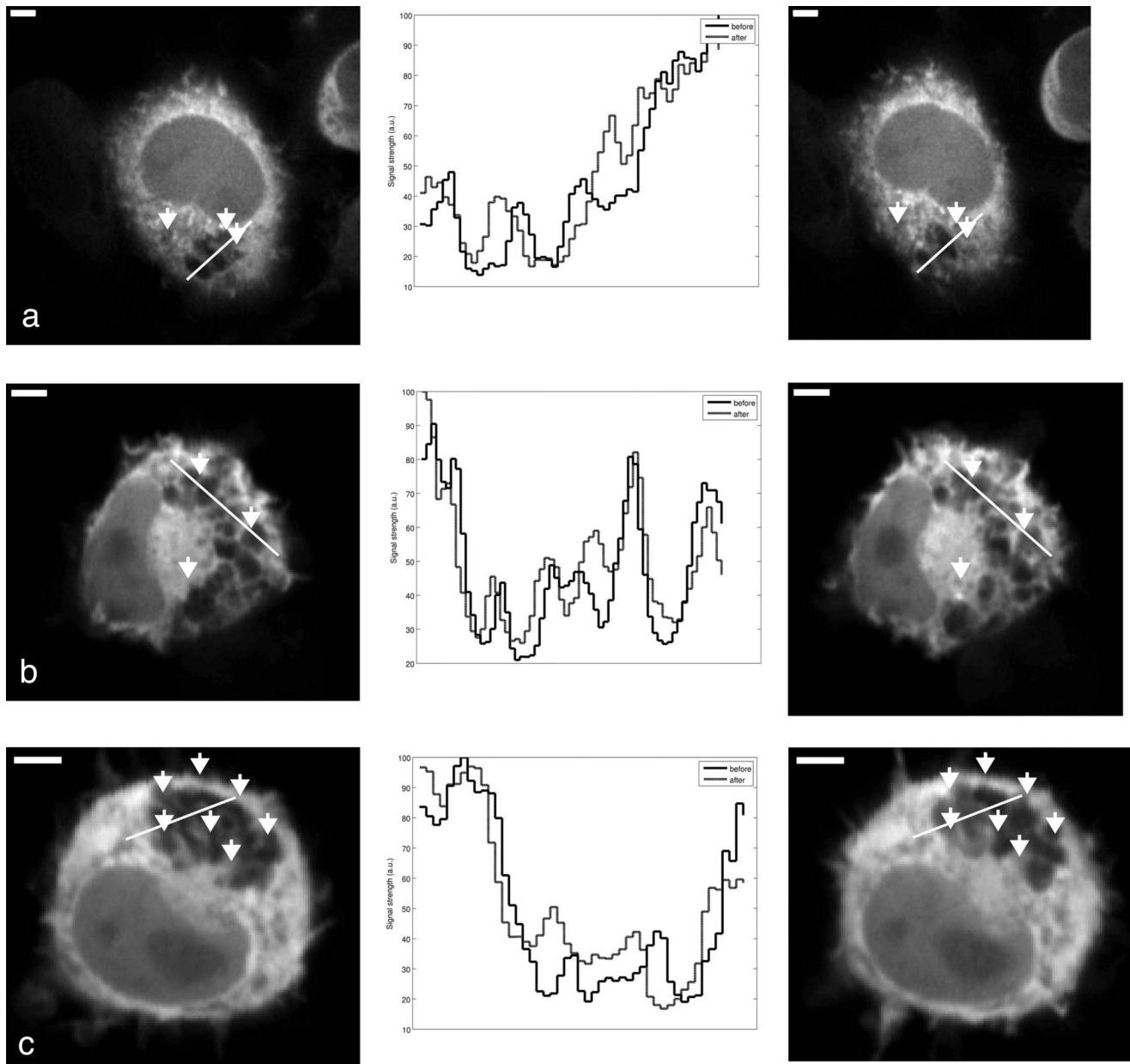


Fig. 8 Images of live *Theileria* parasites within their macrophage host cells; the scale bar in all images is $2\ \mu\text{m}$. The grayscale shading was performed separately for each image (black corresponds to no signal and white to the maximum signal recorded in that image). The images are taken in the plane normal to the incident laser beam in which the laser was focused for ablation. The panels in the left (right) column show the cells before (after) ultrashort pulse laser ablation. The arrows point to the locations where single, tightly focused ultrashort pulses irradiated the sample. The panels in the center column show a plot of a cross section through the corresponding images in the left and right columns. The cross sections are plotted along the white lines indicated in the images. The cross-section plots are both normalized to the maximum signal strength observed in either plot, and the curves can be compared directly (black=before, gray=after). The cell shows no large structural changes, but the parasite is altered in each case; single parasite lobes have filled with GFP. The peak laser intensity used was: (a) $8.8\ \text{TW}/\text{cm}^2$, (b) $19\ \text{TW}/\text{cm}^2$, and (c) $8.6\ \text{TW}/\text{cm}^2$. These peak intensities correspond to pulse energies of: (a) $3.2\ \text{nJ}$, (b) $6.8\ \text{nJ}$, and (c) $3.1\ \text{nJ}$.

about $12\ \text{TW}/\text{cm}^2$ did not result in cell death in any of the experiments. These results are summarized in Table 2, which gives the number of cells that died as a result of laser treatment for different pulse energy ranges, as well as the number of cells in which the parasite was filled.

We confirmed the viability of the cells up to $\sim 5\ \text{h}$ (the maximum time the cells were observed) after laser irradiation both by reimaging selected cells using multiphoton microscopy and—since determination of cell viability does not

require high axial resolution—by observing them using conventional epi-fluorescence microscopy, which allows rapid observation of multiple cells. We used the presence or absence of an intact nucleus and parasite to gauge the viability of the cells.²⁷ Specifically, we found that of 21 cells exposed to laser irradiation without it resulting in an immediately visible change, 20 survived for at least $\sim 5\ \text{h}$ after the exposure; we could not determine the viability of 1 cell (the nucleus retained its shape, but the parasite was no longer visible). For

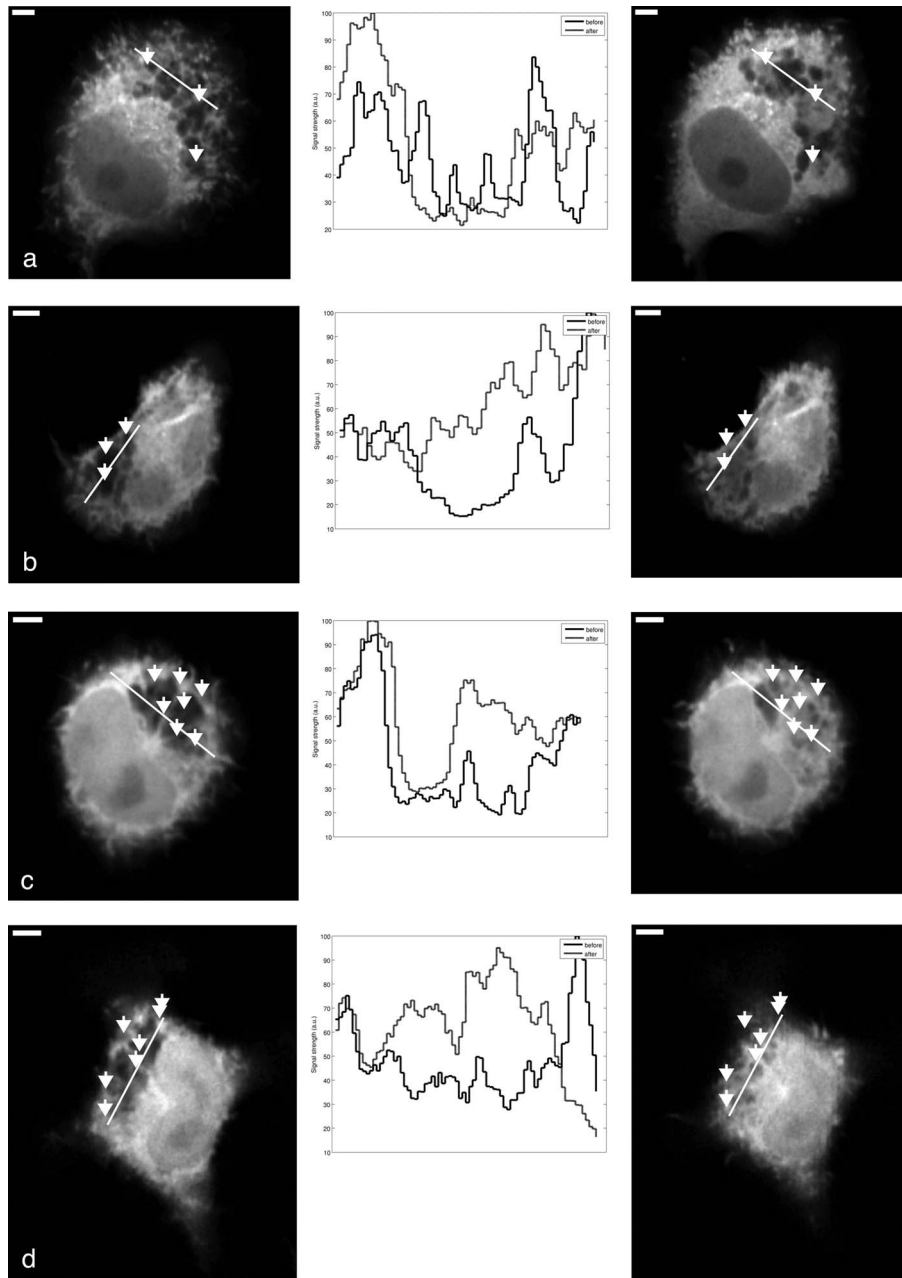


Fig. 9 Images of live *Theileria* parasites within their macrophage host cells; the scale bar in all images is 2 μm . The grayscale shading was performed separately for each image (black corresponds to no signal and white to the maximum signal recorded in that image). The images are taken in the plane normal to the incident laser beam in which the laser was focused for ablation. The panels in the left (right) column show the cells before (after) ultrashort pulse laser ablation. The arrows point to the locations where single, tightly focused ultrashort pulses irradiated the sample. The panels in the center column show a plot of a cross-section through the corresponding images in the left and right columns. The cross sections are plotted along the white lines indicated in the images. The cross-section plots are both normalized to the maximum signal strength observed in either plot, and the curves can be compared directly (black=before, gray=after). The cell shows no large structural changes, but the parasite is significantly altered in each case; GFP has entered not only the parasite lobe that was exposed to the laser, but also neighboring lobes. The peak laser intensity used was: (a) 25 TW/cm^2 , (b) 19 TW/cm^2 , (c) 13 TW/cm^2 , and (d) 13 TW/cm^2 . These peak intensities correspond to pulse energies of: (a) 8.9 nJ, (b) 6.8 nJ, (c) 4.6 nJ, and (d) 4.6 nJ.

the 18 cells that showed an immediately visible change, we observed the following: 5 cells survived for at least ~ 5 h, 7 cells died, and in 6 cases, it was not possible to determine conclusively whether the cell survived using our criteria.

4 Discussion

We used ultrashort pulse laser ablation to generate small holes in the membrane of an intracellular parasite inside its host cell

in living cells as well as in fixed and immunostained cells. Multiphoton microscopy allowed precise 3-D localization of the part of the parasite membrane that was irradiated. It also permitted imaging of resulting structural changes in three dimensions.

In fixed cells in which the parasite membrane had been immunolabeled using Alexa488-conjugated antibodies, we

Table 2 Table of the results of ultrashort pulse laser ablation experiments in living cells. For each peak intensity range, the total number of cells exposed, the number of cells that died, and the number of cells in which the parasite was successfully filled with GFP is provided. Note that the last column in the table does not include cells where the cell died in the process of the parasite being filled with GFP.

Peak laser intensity used for ablation	Number of cells exposed to laser irradiation	Number of cells that died	Number of cells where the parasite was filled with GFP
<12 TW/cm ²	12	0	2
>12 TW/cm ²	11	3	8
Total	23	3	10

observed three distinct intensity regimes with respect to laser ablation. At low enough intensities, the sample was not visibly changed. At intensities between about 9.5 and 19 TW/cm², the degree of damage varied: In some cases, only weak photobleaching of the labeled membrane was observed, while in other cases a visible hole, comparable in size to the focal spot, was generated (no fluorescent signal left at all). In a previous study, it was demonstrated that weak photobleaching of the sample occurs at a laser intensity level approximately 20% below that at which material ablation observable by transmission electron microscopy occurs, and that at laser intensities where the fluorescence is eliminated, material ablation always occurs.²⁸ The variability in the threshold that we observed was in all likelihood due to the fact that the threshold depends on the amount of light scattered out of the laser beam before it reached the focus, which varies from point to point in the sample;²⁹ the ~7% variation in the shot-to-shot pulse energy is too small to account for it. The dye concentration can also influence the threshold in ultrashort pulse laser ablation experiments, but this is more likely to play a role at high-repetition rates (>1 MHz) and lower pulse energies, where accumulated photochemical effects, rather than thermoelastic effects, are responsible for ablation.¹⁸ At even higher intensities, damage to the parasite membrane always occurred and was no longer confined to the focal spot. The threshold intensity ranges we have determined are in good agreement with previous measurements and with numerical simulation of ultrashort pulse laser ablation.¹⁸

The experiments in the fixed cells allowed us to determine the initial extent of ablation in the parasite membrane, without complicating factors such as the parasite's and the cell's response to laser-induced damage. We performed measurements in living *Theileria* parasites inside the host cell in order to elucidate the reaction to laser irradiation and membrane ablation. Laser irradiation at intensities in the same range as that necessary to ablate holes in the fixed, immunostained samples (9.5 to 18 TW/cm²; see Table 1) could lead: (1) to no significant visible changes in the parasite, (2) to a less dark appearance of the parasite lobes against the cytoplasm, (3) to complete destruction of individual lobes of the parasite, and (4) to structural changes—a pronounced change from ellipsoidal to spherical shape—throughout the parasite, including in

lobes that were not directly affected by laser irradiation. Changes in the contrast between a parasite lobe and the surrounding cytoplasm, where GFP is present, were due to the flow of GFP into the parasite when a hole was ablated in the membrane, since photobleaching of the GFP in the cytoplasm—which could also potentially explain such a change in contrast—was found to be negligible. The fact that the parasite lobe appears *brighter* can only be explained by the presence of GFP that has been transported through the membrane.

Laser intensities in the range of <9.5 TW/cm², generally insufficient to produce ablation in the fixed, stained parasites (refer back to Table 1), also did not result in significant changes in the parasite or in cell death (as seen in Table 2). Laser intensities above about 12 TW/cm²—which can be sufficient to perforate the parasite membrane—could also result in death of the parasite and its host cell. Although large variability was observed from cell to cell, increased pulse energy was correlated with an increased likelihood of cell death. Peak intensities above about 50 TW/cm² always led to immediate cell death. Thus, there is a limited range of laser intensities that can be used to allow the movement of GFP from the host cell into the parasite. However, staying near the lower end of the range where perforation of the parasite is possible (say, 12 TW/cm² to 15 TW/cm²) and gradually increasing the intensity if no effect is initially seen allows perforation of the parasite membrane while minimizing the risk of parasite and host cell death. While there is always some risk of cell death when peak intensities sufficiently high to allow GFP to enter the parasite are used, the large majority of cells survive when such a technique is employed.

Structural changes in the parasite were usually visible within seconds after laser irradiation, suggesting that the parasite lobes are tightly interlinked and do not function independently of one another. In some respects, the changes in parasite lobe shape are reminiscent of the fission of lipid vesicles: an elongated lipid vesicle (or, in our case, parasite lobe) undergoes ingression until it finally separates into two more spherical vesicles.³⁰ Even those parasites of which individual lobes were destroyed, or for which all of the lobes acquired a more spherical shape, remained viable during the several hours they were observed. Longer-term studies of parasite and host cell viability would be very useful but are difficult because the parasitized leukocytes move across the glass coverslip and must be tracked during the entire period of study. Modifications of the experimental setup that allow such tracking under optimal cell culture conditions are currently planned.

Our results show that it is possible to generate small holes in the plasma membrane of *Theileria* schizonts residing inside the leukocyte cytoplasm and that both the parasite and the host cell remain viable after laser treatment. This technology may open up new possibilities for transfection of the schizont stage of *Theileria*—something that has not yet been achieved using the currently available methods. Using ultrashort pulse laser ablation, different plasmid constructs designed to express GFP under the control of a parasite-specific promoter, could be tested. Transfection is of fundamental importance to research focused on understanding the mechanisms by which this parasite interacts with its host cell, altering its phenotypic behavior and resulting in uncontrolled proliferation. Although

ultrashort pulse laser transfection has been successfully demonstrated in mammalian cells¹³ and shown to have an efficiency of approximately 50%,¹⁴ the goal of transfecting *Theileria* presents a number of additional new challenges. First, as the half-life of foreign DNA in the cytoplasm is generally only on the order of hours,³¹ the plasmid DNA would need to be introduced into the host cells immediately prior to the laser treatment. This may require microinjection of individual cells after they have attached to the bottom of a glass-bottom dish. Electroporation, a less time-consuming, less labor-intensive, and more efficient technique, requires that the cells be in solution; thus, during the time required for the cells to attach to the glass-bottom dishes (~24 h) before laser treatment, the DNA in the cytoplasm may be destroyed. Second, the actin cytoskeleton of the cell, which hinders movement of large DNA plasmids (>500 kbp), presents an additional major challenge.³² Even if the laser ablates a small region of the parasite membrane, DNA introduced into the host cell cytoplasm may not diffuse efficiently to this region. It remains to be determined whether treatment with Cytochalasin D could be used to depolymerize the actin cytoskeleton, allowing more efficient delivery of plasmid DNA—or potentially also regulatory RNA fragments—into the schizont.

Last, in several cases, the delivery of bioactive compounds such as plant toxins to cells depends on the successful binding to the surface of the cell of a docking subunit, which is left behind when the enzymatically active subunit enters the cell. The absence of the docking subunit inside the host cell precludes the delivery of the bioactive subunit to the cytoplasm of the *Theileria* schizont, but ultrashort pulse laser ablation may now allow such compounds to be delivered to *Theileria*. This, in turn, could be of help to broaden the spectrum of tools available to analyze metabolic and regulatory pathways in the schizont.

Acknowledgments

We thank Prof. J. Rička for helpful discussions and advice. This work was supported in part by a grant from the Swiss National Science Foundation (3152A0-100431).

References

1. P. Leirião, C. D. Rodrigues, S. S. Albuquerque, and M. M. Mota, "Survival of protozoan intracellular parasites in host cells," *EMBO Rep.* **5**, 1142–1147 (2004).
2. A. D. Irvin, C. G. Brown, G. K. Kanhai, and D. A. Stagg, "Comparative growth of bovine lymphosarcoma cells and lymphoid cells infected with *Theileria parva* in athymic (nude) mice," *Nature (London)* **255**, 713–714 (1975).
3. D. A. E. Dobbelaere and P. Küenzi, "The strategies of the *Theileria* parasite: a new twist in host-pathogen interactions," *Curr. Opin. Immunol.* **16**, 524–530 (2004).
4. B. Shiels, G. Langsley, W. Weir, A. Pain, S. McKellar, and D. Dobbelaere, "Alteration of host cell phenotype by *Theileria annulata* and *Theileria parva*: mining for manipulators in the parasite genomes," *Int. J. Parasitol.* **36**, 9–21 (2006).
5. Y. Galley, G. Hagens, I. Glaser, W. C. Davis, M. Eichhorn, and D. A. E. Dobbelaere, "Jun NH2-terminal kinase is constitutively activated in T-cells transformed by the intracellular parasite *Theileria parva*," *Proc. Natl. Acad. Sci. U.S.A.* **94**, 5119–5124 (1997).
6. V. T. Heussler, P. Kuenzi, F. Fraga, R. A. Schwab, B. A. Hemmings, and D. A. E. Dobbelaere, "The Akt/PKB pathway is constitutively activated in *Theileria*-transformed leucocytes but does not directly control constitutive NF-kappaB activation," *Cell. Microbiol.* **3**, 537–550 (2001).
7. V. T. Heussler, S. Rottenberg, R. Schwab, P. Küenzi, P. C. Fernandez, S. McKellar, B. Shiels, Z. Chen, K. Orth, D. Wallach, and D. A. E. Dobbelaere, "Hijacking of host cell IKK signalosomes by the transforming parasite *Theileria*," *Science* **298**, 1033–1036 (2002).
8. G. H. Palmer, J. J. Machado, P. Fernandez, V. Heussler, T. Perinat, and D. A. E. Dobbelaere, "Parasite-mediated nuclear factor μ B regulation in lymphoproliferation caused by *Theileria parva* infection," *Proc. Natl. Acad. Sci. U.S.A.* **96**, 12527–12532 (1997).
9. V. T. Heussler, J. Machado, Jr., P. C. Fernandez, C. Botteron, C. G. Chen, M. J. Pearse, and D. A. E. Dobbelaere, "The intracellular parasite *Theileria parva* protects infected T cells from apoptosis," *Proc. Natl. Acad. Sci. U.S.A.* **96**, 7312–7317 (1999).
10. M. J. Gardner, R. Bishop, T. Shah, E. P. de Villiers, J. M. Carlton, N. Hall, Q. Ren, I. T. Paulsen, A. Pain, M. Berriman, R. J. M. Wilson, S. Sato, S. A. Ralph, D. J. Mann, Z. Xiong, S. J. Shallom, J. Weidman, L. Jiang, J. Lynn, B. Weaver, A. Shoabi, A. R. Domingo, D. Wasawo, J. Crabtree, J. R. Wortman, B. Haas, S. V. Angiuoli, T. H. Creasy, C. Lu, B. Suh, J. C. Silva, T. R. Utterback, T. V. Feldblyum, M. Pertea, J. Allen, W. C. Nierman, E. L. N. Taracha, S. L. Salzberg, O. R. White, H. A. Fitzhugh, S. Morzaria, J. C. Fraser, and V. Nene, "Genomic sequence of *Theileria parva*, a bovine pathogen that transforms lymphocytes," *Science* **309**, 134–137 (2005).
11. A. Pain, H. Renaud, M. Berriman, L. Murphy, C. A. Yeats, W. Weir, A. Kerhormou, M. Aslett, R. Bishop, C. Bouchier, M. Cochet, R. M. R. Coulson, A. Cronin, E. P. de Villiers, A. Fraser, N. Fosker, M. Gardner, A. Goble, S. Griffith-Jones, D. E. Harris, F. Katzer, N. Larke, A. Lord, P. Maser, S. McKellar, P. Mooney, F. Morton, V. Nene, S. O'Neil, C. Price, M. A. Quail, E. Rabbinowitsch, N. D. Rawlings, S. Rutter, D. Saunders, K. Seeger, T. Shah, R. Squares, A. Tivey, A. R. Walker, J. Woodward, D. A. E. Dobbelaere, G. Langsley, M.-A. Rajandream, D. McKeever, B. Shiels, A. Tait, B. Barrell, and N. Hall, "Genome of the host-cell transforming parasite *Theileria annulata* compared with *T. parva*," *Science* **309**, 131–133 (2005).
12. R. Adamson, K. Lyons, M. Sharrard, J. Kinnaird, D. Swan, S. Graham, B. Shiels, and R. Hall, "Transient transfection of *Theileria annulata*," *Mol. Biochem. Parasitol.* **114**, 53–61 (2001).
13. U. K. Tirlapur and K. König, "Targeted transfection by femtosecond laser," *Nature (London)* **418**, 290–291 (2002).
14. D. Stevenson, B. Agate, X. Tsampoula, P. Fischer, C. T. A. Brown, W. Sibbett, A. Riches, F. Gunn-Moore, and K. Dholakia, "Femtosecond optical transfection of cells: viability and efficiency," *Opt. Express* **14**, 7125–7133 (2006).
15. W. R. Zipfel, R. M. Williams, and W. W. Webb, "Nonlinear magic: multiphoton microscopy in the biosciences," *Nat. Biotechnol.* **21**, 1369–1377 (2003).
16. B. R. Masters, *Confocal Microscopy and Multiphoton Excitation Microscopy: The Genesis of Live Cell Imaging*, Monograph Vol. PM161, SPIE Press, Bellingham, WA (2006).
17. K. König, I. Riemann, and W. Fritzsche, "Nanodissection of human chromosomes with near-infrared femtosecond laser pulses," *Opt. Lett.* **26**, 819–821 (2001).
18. A. Vogel, J. Noack, G. Hüttman, and G. Paltauf, "Mechanisms of femtosecond laser nanosurgery of cells and tissues," *Appl. Phys. B* **81**, 1015–1047 (2005).
19. J. A. Galbraith and M. Terasaki, "Controlled damage in thick specimens by multiphoton excitation," *Mol. Biol. Cell* **14**, 1808–1817 (2003).
20. F. H. Loesel, J. P. Fischer, M. H. Götz, C. Horvath, T. Juhasz, F. Noack, N. Suhm, and J. F. Bille, "Nonthermal ablation of neural tissue with femtosecond laser pulses," *Appl. Phys. B* **66**, 121–128 (1998).
21. W. Watanabe, N. Arakawa, S. Matsunaga, T. Higashi, K. Fukui, K. Isobe, and K. Itoh, "Femtosecond laser disruption of subcellular organelles in a living cell," *Opt. Express* **12**, 4203–4213 (2004).
22. N. Shen, D. Dabajyoti, C. B. Schaffer, P. LeDuc, D. E. Ingber, and E. Mazur, "Ablation of cytoskeletal filaments and mitochondria in live cells using a femtosecond laser nanoscissor," *Mech. Chem. Biosyst.* **2**, 17–25 (2005).
23. W. Supatto, D. Débarre, B. Moulia, E. Brouzés, J.-L. Martin, E. Farge, and E. Beaurepaire, "In vivo modulation of morphogenetic movements in *Drosophila* embryos with femtosecond laser pulses," *Proc. Natl. Acad. Sci. U.S.A.* **102**, 1047–1052 (2005).
24. M. Kauert, M. J. Rička, and M. Frenz, "Characterization and preparation of focused laser beams," *Opt. Eng.* **47**, 014201 (2008).
25. L. Schnittger, F. Katzer, R. Biermann, P. Shayan, K. Boguslawski, S. McKellar, D. Beyer, B. R. Shiels, and J. S. Ahmed, "Characterization

- of a polymorphic *Theileria annulata* surface protein (TaSP) closely related to PIM of *Theileria parva*: implications for use in diagnostic tests and subunit vaccines," *Mol. Biochem. Parasitol.* **120**, 247–256 (2002).
26. K. König, T. W. Becker, P. Fischer, I. Riemann, and K.-J. Halhuber, "Pulse-length dependence of cellular response to intense near-infrared laser pulses in multiphoton microscopes," *Opt. Lett.* **24**, 113–115 (1999).
 27. C. S. Potten and J. Wilson, *Apoptosis—The Life and Death of Cells*, Cambridge University Press, Cambridge, UK (2004).
 28. A. Heisterkamp, I. Z. Maxwell, E. Mazur, J. M. Underwood, J. A. Nickerson, S. Kumar, and D. E. Ingber, "Pulse energy dependence of subcellular dissection by femtosecond laser pulses," *Opt. Express* **13**, 3690–3693 (2005).
 29. N. I. Smith, K. Fujita, O. Nakamura, and S. Kawata, "Three-dimensional subsurface microprocessing of collagen by ultrashort laser pulses," *Appl. Phys. Lett.* **78**, 999–1001 (2001).
 30. H. G. Döbereiner, J. Käs, D. Noppl, I. Sprenger, and E. Sackmann, "Budding and fission of vesicles," *Biophys. J.* **65**, 1396–1403 (1993).
 31. D. Lechardeur and G. L. Lukacs, "Nucleocytoplasmic transport of plasmid DNA: a perilous journey from the cytoplasm to the nucleus," *Hum. Gene Ther.* **17**, 882–889 (2006).
 32. E. Dauty and A. S. Verkman, "Actin cytoskeleton as the principal determinant of size-dependent DNA mobility in cytoplasm: a new barrier for nonviral gene delivery," *J. Biol. Chem.* **280**, 7823–7828 (2005).